

# Journal of Biomedical Optics

BiomedicalOptics.SPIEDigitalLibrary.org

## **Multimodality Raman and photoacoustic imaging of surface- enhanced-Raman-scattering-targeted tumor cells**

Wei Shi  
Robert J. Paproski  
Peng Shao  
Alexander Forbrich  
John D. Lewis  
Roger J. Zemp

**SPIE.**

# Multimodality Raman and photoacoustic imaging of surface-enhanced-Raman-scattering-targeted tumor cells

Wei Shi,<sup>a</sup> Robert J. Paproski,<sup>a,b</sup> Peng Shao,<sup>a</sup> Alexander Forbrich,<sup>a</sup> John D. Lewis,<sup>b</sup> and Roger J. Zemp<sup>a,\*</sup>

<sup>a</sup>University of Alberta, Department of Electrical and Computer Engineering, Second Floor ECERF, 9107-116 Street, Edmonton, Alberta, T6G 2V4, Canada

<sup>b</sup>University of Alberta, Department of Oncology, 114 Street and 87 Avenue, Edmonton, Alberta, T6G 2E1, Canada

**Abstract.** A multimodality Raman and photoacoustic imaging system is presented. This system has ultralow background and can detect tumor cells labeled with modified surface-enhanced-Raman-scattering (SERS) nanoparticles *in vivo*. Photoacoustic imaging provides microvascular context and can potentially be used to guide magnetic trapping of circulating tumor cells for SERS detection in animal models. © The Authors. Published by SPIE under a Creative Commons Attribution 3.0 Unported License. Distribution or reproduction of this work in whole or in part requires full attribution of the original publication, including its DOI. [DOI: [10.1117/1.JBO.21.2.020503](https://doi.org/10.1117/1.JBO.21.2.020503)]

**Keywords:** multimodality imaging; Raman spectroscopy; surface-enhanced Raman scattering; nanoparticles; photoacoustic; biomedical optics.

Paper 150833LR received Dec. 15, 2015; accepted for publication Jan. 26, 2016; published online Feb. 25, 2016.

Specific and sensitive detection of individual tumor cells *in vivo* with ultralow background detection is challenging despite many recent attempts.<sup>1–13</sup> Fluorescence-based detection suffers from significant background autofluorescence.<sup>14</sup> Bioluminescence offers ultralow background but requires genetic prelabeling of cells.<sup>15</sup> Photoacoustic flow cytometry has identified circulating melanoma cells or nanoparticle-labeled nonpigmented tumor cells, but endogenous hemoglobin gives a non-negligible background.<sup>3,4,10,11</sup> Recently, surface-enhanced Raman-scattering (SERS) nanoparticles have been under investigation as a promising labeling agent.<sup>7–9,16</sup> These SERS nanoparticles exhibit a spectral fingerprint unique to their Raman-reporter on a metallic nanocore and encapsulated by a silica layer. These bright spectral barcodes have shown significant promise for multiplexed molecular imaging but also have the advantage of ultralow background, allowing sensitive and specific detection. Multimodality SERS, photoacoustic, and MRI imaging were previously reported for solid tumor imaging;<sup>16</sup> however,

in their studies, single-cell detection was not reported, nor was application for circulating tumor cell (CTC) detection, although photoacoustic detection of single melanoma CTC was reported in Ref. 12. A dual-modality microscopy integrating photoacoustic microscopy (PAM) and fluorescence confocal microscopy were developed to image hemoglobin oxygen saturation (sO<sub>2</sub>) and oxygen partial pressure (pO<sub>2</sub>) *in vivo* in single blood vessels with high spatial resolution. However, they did not demonstrate the capability to detect CTCs.<sup>17</sup> Recently, we demonstrated SERS-based detection of magnetically trapped CTCs *in vitro*.<sup>13</sup> Here we extend this work to include a multimodality photoacoustic-SERS imaging platform and to demonstrate ultralow-background Raman-detection of SERS-targeted tumor cells *in vivo*. The PAM subsystem enables detailed visualization of the microvascular structure and potentially can guide the placement of a trapping magnet. The SERS subsystem is capable of detecting single tumor cells if they are targeted with more than 200 SERS nanoparticles per cell.<sup>13</sup>

To target widely overexpressed folate receptors on cancer cells, we conjugated both SERS nanoparticles (S440 & S421, BD Technologies) and magnetic fluorescent silica particles (screenMAG-Thiol, chemicell GmbH) with folate.<sup>13</sup> Simply, folate-PEG5k-maleimide (0.8 mM, PG2-FAML-5k, Nanocs Inc.) and methoxy-PEG2k-maleimide (4 mM, Sigma Aldrich) were added to thiolated SERS nanoparticle solution (1.3 nM, a 60 nm diameter Au core, and a 30 nm silica shell). After mixing and rocking the solution overnight at room temperature, excess folate-PEG-maleimide was removed by three runs of centrifugation (14,000 RPM, 5 min). Similar process was applied to magnetic nanoparticles (1.25 nM, 500 nm diameter magnetic fluorescent silica particles).

The diagram of our imaging system is demonstrated in Fig. 1. A 785 nm Raman laser RL (FB-785-350-FS-FS-1-1, RGLase LLC) with 0.4 nm 20 dB spectral line-width and up to 350 mW output (while the power used in our experiment was 54 mW) was used as excitation laser source for SERS imaging. The excitation laser beam transmitted through a dichroic beam splitter BS (DMSP805L, Thorlabs) toward mirror M and was then focused onto sample by an aspheric lens L2 (A240TM-B, Thorlabs, 0.5 NA, 8 mm focal length) with large NA to enable high collection efficiency needed for sensitive SERS detection. Sample was placed on a three-axis translation stage, controlled by a four-axis PCI stepper/servo motion controller (NI PCI-7354, National Instruments). A 1 in. tall, 1 in. diameter N50 cone magnet (Cone0100N, SuperMagnetMan) was pointed at the sample, generating strong magnetic field with high magnetic field gradient for magnetic trapping. SERS generated by sample was collected by lens L2, reflected by mirror M, and beam splitter BS. A 0.3 NA lens (AC127-019-B-ML, Thorlabs) focused SERS beam into a custom Raman imaging spectrometer (RASPEEC-785-HR, P&P Optica Inc.), with a 15 μm × 26 mm slit as input aperture (f#: 3.5). A 10 cm<sup>-1</sup> spectral resolution within spectral range of 815 to 895 nm was obtained using a 900 1/cm gel-grating in the Raman imaging spectrometer. A liquid-cooled electron-multiplying (EM) CCD camera (DU971N-UV, Andor Technology) was implemented for detection and signal acquisition, with very low dark current noise (0.0002 e<sup>-</sup>/pix/s at -100°C) and ~50% quantum efficiency at peak wavelengths, ~30% in the wavelength range we used. There were 1600 × 400 pixels on the EMCCD array, with 16 × 16 μm element size. The EM gain was set at 10, integration time was 1 s, and sensor temperature was liquid

\*Address all correspondence to: Roger J. Zempa, E-mail: [rzemp@ualberta.ca](mailto:rzemp@ualberta.ca)

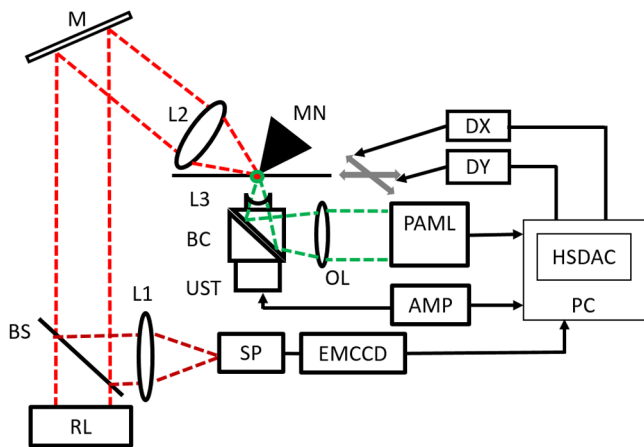


**Fig. 1** Experiment setup for the multimodality imaging system. RL, Raman laser; BS, beam splitter; L1, lens 1; SP, spectrometer; M, mirror; L2, lens 2; MN, magnet; L3, lens 3; BC, beam combiner; UST, ultrasonic transducer; OL, objective lens; DX, DY, XY translation stage drivers; PAML, PAM laser; AMP, amplifier; HSDAC, high speed data acquisition card; PC, personal computer.

cooled to  $-100^{\circ}\text{C}$ . SERS signals were finally acquired by imaging software (SOLIS, Andor Technology Ltd.). A custom-designed PAM probe was placed on the side of the sample opposite from lens L2 and magnet MN to achieve PAM imaging. The 10 Hz 532 nm laser pulses were generated by a Q-switch laser source (ND6000, Continuum) and was focused by an objective lens (M Plan Apo,  $5\times$ ,  $\text{NA} = 0.14$ ,  $f = 20$  cm, Edmund Optics Inc.). A beam combiner consist of a 15 mm aluminum-coated prism (BRAP15-A, Newport Co.) and a 15 mm uncoated prism (RA 15 mm UNCTD TS, Edmund Optics Inc.) was used for reflecting 532 nm laser beam onto the sample, while transmitting generated photoacoustic signals from sample to a 50 MHz ultrasound transducer (V214-BB-RM, Olympus Corp.) for acoustic detection. An acoustic lens L3 ( $f = 6$  mm,  $\text{NA} = 0.5$ , Edmund Optics Inc.) is attached to the top surface of the beam combiner. Received photoacoustic signals were then amplified by an ultrasound pulser-receiver (5900PR, Olympus NDT Inc.). A high speed data acquisition card (CS8289, Gage Cobra, Gage Applied Systems, Inc.) with 12-bit dynamic range and up to 125 MSamples/s sample rate acquired the PAM laser trigger, the feedback positions of the translation stages, and the photoacoustic signals.

In our experiment, Raman imaging of folate-receptor over-expressing HeLa cells (cervical cancer and folate receptor positive) was performed by labeling HeLa cells with SERS and magnetic nanoparticles (which were both folate-conjugated), magnetically trapping cells in the focal zone of lens 2, and acquiring SERS signals from the magnetic focal zone.<sup>13</sup> Simply, we took SERS spectrum from the SERS nanoparticle solution as a reference spectrum, which was then used for demixing of SERS spectrum obtained from all samples by implementing a classic linear least-squares method with an optional positivity constrain to quantify SERS signals. A concentration unit was used in Ref. 13 for simple comparison. Further data processing and analysis were conducted by MATLAB programs (Mathworks, Inc.) in the data acquisition computer.

In our Raman and photoacoustic imaging system, the Raman imaging subsystem works similar to the single modality Raman imaging system described in our previous publication,<sup>13</sup> with

$\sim 1$  pM SERS nanoparticle detection sensitivity, single-cell detection capability, high multiplexing ability, and 1 : 12 nonspecific binding ratio reported between HeLa and ZR-75-1 cell lines. Very little false-positive signal was observed from blood cells. For *in vitro* detection of CTCs, we used two types of nanoparticles: folate-receptor-targeted SERS nanoparticles and folate-receptor-targeted magnetic nanoparticles. Only cells targeted with both SERS and magnetic nanoparticles were trapped and detected. Previous work, however, used prelabeled tumor cells, did not demonstrate *in vivo* imaging and lacked another modality for spatial registration. The present work incorporates a photoacoustic imaging subsystem, investigates trapping of CTCs without prelabeling, and illustrates *in vivo* imaging and CTC detection.

In phantom studies, after incubating with serum-free medium containing folate-conjugated SERS nanoparticles and magnetic nanoparticles at  $37^{\circ}\text{C}$  for 4 h,  $\sim 5 \times 10^4$  HeLa cells were mixed with 1 mL rat blood, flowing inside a  $200\ \mu\text{m}$  inner-diameter acrylic capillary tubing (CT200-250-5, Paradigm Optics) at 3 cm/s flow velocity controlled by a syringe pump (NE-300, New Era Pump Systems, Inc.). Figure 2(a) shows a 1 mm  $\times$  1 mm coregistered Raman and photoacoustic image of rat blood mixed with SERS/magnetic nanoparticle-labeled HeLa cells flowing and magnetically trapped inside tubing. The cone magnet pointed at the lower left corner of the image. PAM and SERS signals are demonstrated in red and blue pseudocolor maps, respectively. The lateral resolution of the PAM imaging subsystem was measured as  $\sim 50\ \mu\text{m}$  by imaging a  $\sim 7.5\ \mu\text{m}$  carbon fiber.<sup>18</sup>

To further demonstrate the capability of applying our method for the detection of CTCs under native targeting process, instead of incubating HeLa cells with nanoparticles before imaging, we first mixed HeLa cells with rat blood, and then added with folate-conjugated SERS nanoparticles and magnetic nanoparticles. HeLa cells ( $\sim 1 \times 10^5$  or  $\sim 5 \times 10^4$ ) were first mixed with 1 mL rat blood for 10 min. Rat blood (1 mL) without HeLa cells was used as a control. The three groups of rat blood samples were then incubated with folate-conjugated SERS nanoparticles ( $\sim 0.4$  nM,  $20\ \mu\text{L}$ ) and magnetic nanoparticles ( $\sim 0.4$  nM,  $20\ \mu\text{L}$ ) before flowing the samples inside a  $200\ \mu\text{m}$  inner-diameter acrylic capillary tubing at 3 cm/s flow velocity. Detected SERS signal versus magnetic trapping time is plotted in Fig. 2(b). Rat blood samples mixed with HeLa cells exhibited increasing SERS signals with magnetic trapping time, while SERS signals from rat blood sample without HeLa cells stayed close to the detection limit of our system throughout the experiment. This demonstrated specific targeting of folate-conjugated nanoparticles to folate receptor positive HeLa cells.

For *in vivo* studies, experimental animal procedures were conducted in conformity with the laboratory animal protocol which is approved by the University of Alberta Animal Use and Care Committee. A breathing anesthesia system (E-Z Anesthesia, Euthanex Corp.) was used to anesthetize the rats for imaging with isoflurane during image acquisition. After incubated with serum-free medium-containing folate-conjugated SERS and magnetic nanoparticles at  $37^{\circ}\text{C}$  for 4 h,  $\sim 5 \times 10^5$  HeLa cells were mixed with  $50\ \mu\text{L}$  PBS solution. The solution was then subcutaneously injected into a rat ear. Figure 3(a) shows a 7 mm  $\times$  7 mm rat ear vasculature imaging by PAM, and co-registered Raman imaging of injected HeLa cells, with pseudocolor to illustrate PAM and SERS signals in red and blue color maps, respectively.

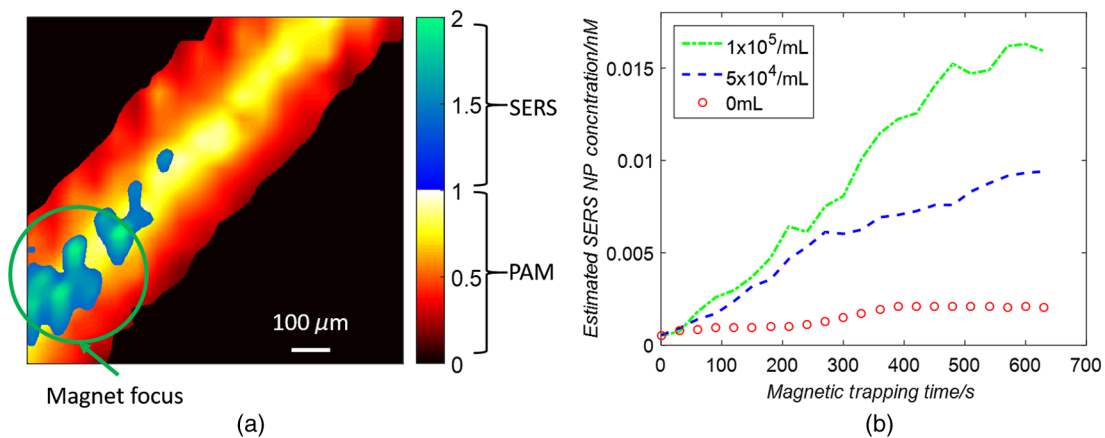


**Fig. 2** Phantom studies: (a) 1 mm × 1 mm co-registered Raman and photoacoustic imaging of rat blood mixed with SERS and magnetic nanoparticle-targeted HeLa cells flowing and magnetically trapped inside a 200 μm inner-diameter acrylic capillary tubing at 3 cm/s flow velocity. PAM and SERS signals are demonstrated in red and blue pseudocolor color maps, respectively; (b) magnetic trapping and SERS detection of HeLa cells in rat blood flowing inside a 200 μm inner-diameter acrylic capillary tubing at 3 cm/s flow velocity. Estimated SERS nanoparticle concentration detected at focal zone at different magnetic trapping time. Rat blood with different HeLa cell concentrations was studied: 10<sup>5</sup>/mL, 5 × 10<sup>4</sup>/mL, and 0/mL.

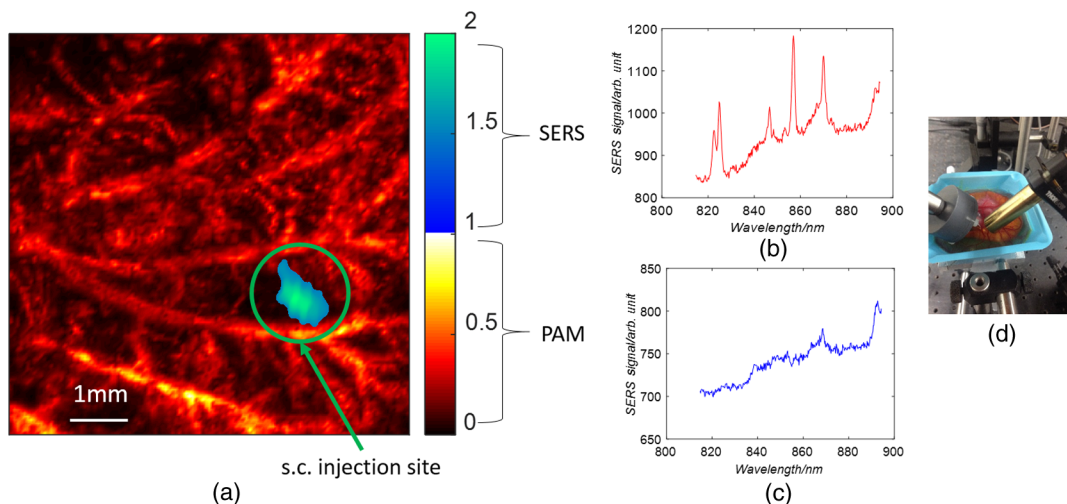


**Fig. 3** *In vivo* studies: (a) 7 mm × 7 mm rat ear vasculature imaging by photoacoustic imaging, and co-registered Raman imaging of injected targeted-HeLa cells, with pseudocolor to illustrate PAM and SERS signals in red and blue color maps, respectively. (b) SERS signal spectrum obtained from magnetic trapping region of chicken embryo membrane, (c) spectrum obtained away from magnetic trapping region, and (d) a photograph of magnetic trapping and SERS detection setup using chicken embryo, respectively.

In our experiments, the Raman excitation laser power of 54 mW is slightly less than that of 60 mW reported by the other group.<sup>7,8</sup> In our *in vivo* experiment with rat ear, to avoid over exposure to the skin, the laser beam was scanned over a 7 mm × 7 mm illuminated area to acquire imaging. Therefore, the corresponding power density by Raman excitation laser used was ~0.11 W/cm<sup>2</sup>, which is under the suggested ANSI maximum permissible exposure limit of 0.2 mW/cm<sup>2</sup> for a 785 nm laser with an exposure duration time from 10 s to 8 h. In addition, no apparent skin burns of mice were observed after laser exposure.

To demonstrate the ability to detect magnetically trapped CTCs, we injected ~1 × 10<sup>5</sup> HeLa cells into the chorioallantoic membrane of an *ex ovo* chicken embryo. The cells were

prelabeled with both SERS and magnetic nanoparticles. A cone magnet was used for magnetic trapping over large vessels away from the injection point. The vessels used for trapping were visible by eye (such placement is not typically possible in many other organisms with highly scattering skin and tissues, hence the value of the photoacoustic subsystem). The Raman subsystem was used to detect the accumulation of magnetically trapped tumor cells labeled with SERS nanoparticles. While no signal was apparent initially, after 10 min, detectable SERS signatures were visible in the trapping region, but not in areas away from the trapping zone. With only SERS or only magnetic nanoparticles, no accumulated SERS signals were measurable, consistent with our previous work. Figures 3(b), 3(c), and 3(d) show the SERS signal spectrum obtained from the magnetic trapping

region, the spectrum obtained away from the magnetic trapping region, and a photograph of magnetic trapping and SERS detection setup with a chicken embryo, respectively.

In summary, we demonstrated the capability of our multimodality SERS and photoacoustic system to specifically trap and detect CTCs *in vitro* without pretargeting and, to detect trapped CTCs *in vivo*, and to provide structural information of surrounding vasculature. We previously determined  $\sim$ pM sensitivities of the Raman detection system. If cells are labeled with more than 200 SERS nanoparticles, single-cell detection is thus possible. Present work focuses on Raman detection of magnetically trapped CTCs. Similar to previous work, photoacoustic imaging could also be used for CTC detection; however, a higher repetition-rate laser may be required. Presently with a 10 Hz laser current imaging time of our system is limited to 160 s for a  $2 \times 2$  mm field of view. Future work would be to combine Raman excitation laser beam with photoacoustic excitation beam so as to co-focus on the sample from the same side of the sample, which will enable applying this system further to imaging thick targets in reflection mode. This technique could be used for studying or detection of CTCs, providing molecular information along with structural or functional vasculature imaging. We believe that the current study offers critical feasibility data to motivate future work on creating new multimodality imaging tools.

### Acknowledgments

The authors gratefully acknowledge funding from a Prostate Cancer Canada Movember Discovery Grant, NSERC (355544-2008, 375340-2009, STPGP 396444), the Canadian Cancer Society (CCS 2011-700718), the Canada Foundation for Innovation, Leaders Opportunity Fund (18472), Alberta Advanced Education & Technology, Small Equipment Grants Program (URSI09007SEG), Alberta Ingenuity and Alberta Innovates scholarships for graduate students, Alberta Innovates Technology Futures Postdoctoral Fellowship Program, Canadian Federation of University Women Edmonton Margaret Brine Graduate Scholarships for Women and SPIE Optics and Photonics Education Scholarship.

### References

1. D. E. Jenkins et al., "Bioluminescent human breast cancer cell lines that permit rapid and sensitive *in vivo* detection of mammary tumors and multiple metastases in immune deficient mice," *Breast Cancer Res.* **7**, R444–R454 (2005).
2. L. Yan et al., "A versatile activatable fluorescence probing platform for cancer cells *in vitro* and *in vivo* based on self-assembled aptamer/carbon nanotube ensembles," *Anal. Chem.* **86**, 9271–9277 (2014).
3. E. I. Galanzha et al., "In vivo, noninvasive, label-free detection and eradication of circulating metastatic melanoma cells using two-color photoacoustic flow cytometry with a diode laser," *Cancer Res.* **69**, 7926–7934 (2009).
4. V. P. Zharov et al., "In vivo photoacoustic flow cytometry for monitoring of circulating single cancer cells and contrast agents," *Opt. Lett.* **31**(24), 3623–3625 (2006).
5. P. Z. McVeigh et al., "Widefield quantitative multiplex surface enhanced Raman scattering imaging *in vivo*," *J. Biomed. Opt.* **18**(4), 046011 (2013).
6. Y. W. Wang et al., "In vivo multiplexed molecular imaging of esophageal cancer via spectral endoscopy of topically applied SERS nanoparticles," *Biomed. Opt. Express* **6**(10), 3714–3723 (2015).
7. C. L. Zavaleta et al., "Multiplexed imaging of surface enhanced Raman scattering nanotags in living mice using noninvasive Raman spectroscopy," *Proc. Natl. Acad. Sci. U. S. A.* **106**(32), 13511–13516 (2009).
8. S. Keren et al., "Noninvasive molecular imaging of small living subjects using Raman spectroscopy," *Proc. Natl. Acad. Sci. U. S. A.* **105**(15), 5844–5849 (2008).
9. X. Wang et al., "Detection of circulating tumor cells in human peripheral blood using surface-enhanced Raman scattering nanoparticles," *Cancer Res.* **71**(5), 1526–1532 (2011).
10. C. M. Obrien et al., "Capture of circulating tumor cells using photoacoustic flowmetry and two phase flow," *J. Biomed. Opt.* **17**, 061221 (2012).
11. Y. Wang et al., "Fiber-laser-based photoacoustic microscopy and melanoma cell detection," *J. Biomed. Opt.* **16**, 011014 (2011).
12. L. Wang et al., "Photoacoustic imaging of single circulating melanoma cells *in vivo*," *Proc. SPIE* **9323**, 93230A (2015).
13. W. Shi et al., "Detection of circulating tumor cells using targeted surface-enhanced Raman scattering nanoparticles and magnetic enrichment," *J. Biomed. Opt.* **19**(5), 056014 (2014).
14. J. Rao, A. Dragulescu-Andrasi, and H. Yao, "Fluorescence imaging *in vivo*: recent advances," *Curr. Opin. Biotechnol.* **18**, 17–25 (2007).
15. G. Vassaux and T. Groot-Wassink, "In vivo noninvasive imaging for gene therapy," *J. Biomed. Biotechnol.* **2003**, 92–101 (2003).
16. M. F. Kircher et al., "A brain tumor molecular imaging strategy using a new triple-modality MRI-photoacoustic-Raman nanoparticle," *Nat. Med.* **18**, 829–834 (2012).
17. Y. Wang et al., "In vivo integrated photoacoustic and confocal microscopy of hemoglobin oxygen saturation and oxygen partial pressure," *Opt. Lett.* **36**, 1029–1031 (2011).
18. W. Shi et al., "Optical resolution photoacoustic microscopy using novel high-repetition-rate passively Q-switched microchip and fiber lasers," *J. Biomed. Opt.* **15**, 056017 (2010).